Chaotic dynamics and control of deterministic ratchets

2005 J. Phys.: Condens. Matter 17 S3719

(http://iopscience.iop.org/0953-8984/17/47/006)

INSTITUTE OF PHYSICS PUBLISHING JOURNAL OF PHYSICS: CONDENSED MATTER

J. Phys.: Condens. Matter **17** (2005) S3719–S3739 doi:10.1088/0953-8984/17/47/006

Chaotic dynamics and control of deterministic ratchets

Fereydoon Family[1,3], **H A Larrondo**[2], **D G Zarlenga**[2] **and C M Arizmendi**[1,2]

[1] Department of Physics, Emory University, Atlanta, GA 30322, USA
[2] Departamento de Física, Facultad de Ingeniería, Universidad Nacional de Mar del Plata, Avenida JB Justo 4302, 7600 Mar del Plata, Argentina

E-mail: phyff@emory.edu

Received 12 September 2005
Published 4 November 2005
Online at stacks.iop.org/JPhysCM/17/S3719

Abstract

Deterministic ratchets, in the inertial and also in the overdamped limit, have a very complex dynamics, including chaotic motion. This deterministically induced chaos mimics, to some extent, the role of noise, changing, on the other hand, some of the basic properties of thermal ratchets; for example, inertial ratchets can exhibit multiple reversals in the current direction. The direction depends on the amount of friction and inertia, which makes it especially interesting for technological applications such as biological particle separation. We overview in this work different strategies to control the current of inertial ratchets. The control parameters analysed are the strength and frequency of the periodic external force, the strength of the quenched noise that models a non-perfectly-periodic potential, and the mass of the particles. Control mechanisms are associated with the fractal nature of the basins of attraction of the mean velocity attractors. The control of the overdamped motion of noninteracting particles in a rocking periodic asymmetric potential is also reviewed. The analysis is focused on synchronization of the motion of the particles with the external sinusoidal driving force. Two cases are considered: a perfect lattice without disorder and a lattice with noncorrelated quenched noise. The amplitude of the driving force and the strength of the quenched noise are used as control parameters.

(Some figures in this article are in colour only in the electronic version)

1. Introduction

The nonequilibrium mechanism of generating net currents, in the absence of bias, from fluctuations interacting with broken symmetry structures, has recently received much attention [1–3]. Feynman *et al* [4] introduced the *ratchet* idea, basically a spatially asymmetric potential, to show the fundamental property of detailed balance that forbids the possibility

[3] Author to whom any correspondence should be addressed.

0953-8984/05/473719+21$30.00

of nonzero net current at the thermodynamic equilibrium. On the other hand, if detailed balance is broken and the substrate potential is asymmetric, a nonzero net drift has been observed in the absence of any macroscopic gradient of forces [5]. This interest is due to the possible applications of these models for understanding such systems as molecular motors [2, 3], nanoscale friction [6], surface smoothening [7], coupled Josephson junctions [8], mass separation and trapping schemes at the microscale [9]. The fluctuations that produce the net transport are usually associated with noise, but they may also arise in the absence of noise, with additive forcing, in overdamped deterministic systems [10], overdamped quenched systems [11] and underdamped ones [12–15].

Molecular motors are individual protein molecules that are responsible for essentially all internal biomaterial transport. They perform tasks vital to the life of the organism like muscle contraction, intracellular transport and cell division. The ratchet model has helped to understand how molecular motors operate [2, 3].

Thermal ratchets have mainly been used to model molecular motors. Nevertheless, deterministic ratchets [11–15] may be used to model molecular motors in some cases because the periodic and chaotic forces associated with deterministic ratchets can lead to directed transport, even in the absence of thermal fluctuations. A possible example of deterministic ratchet application may be molecular motors in muscles that have linear structures, which consist of many parts that supply intrinsic degrees of freedom essential for net motion to occur. Also the two-headed kinesin direction of motion along microtubules could be reversed by adjusting the architecture of a small part of the molecular motor called the neck region [16, 17]. In these examples the existence of a net current depends less on the position thermal fluctuations produced by a noisy environment, while intrinsic structures and symmetry properties of the system may play a more important role in producing directed transport. Recently, stochastic ratchet models were proposed characterized (i) by a spatial coordinate x which describes the displacement of the motor molecule along the filament, (ii) by M internal states, which represent the various conformations the molecule can attain for a fixed value of x, and (iii) by K spatial positions per motor cycle at which the motor molecule can undergo transitions between these different internal states [18].

Inertial ratchets, even in the absence of noise, have a very complex dynamics, including chaotic motion [12]. This deterministically induced chaos mimics, to some extent, the role of noise [19], changing, on the other hand, some of the basic properties of thermal ratchets, for example, inertial ratchets can exhibit multiple reversals in the current direction [12, 13]. The direction depends on the amount of friction and inertia, which makes it especially interesting for technological applications such as biological particle separation [9].

The dynamical current reversal in deterministic systems has been studied in detail recently. Jung *et al* [12] studied the case of an underdamped particle periodically driven in an asymmetric potential without noise and found multiple current reversals varying the intensity of the external perturbation. They characterized the motion by cumulants of the contracted, time-dependent solution of the Liouville equation and distinguished regular from chaotic transport. Mateos [13] analysed the relation between the bifurcation diagram and the current. He conjectured that the origin of the current reversal is the bifurcation from a chaotic to a periodic regime. Close to this bifurcation he observed trajectories revealing intermittent chaos and anomalous deterministic diffusion. Barbi *et al* [14] related the transport properties to phase locking dynamics. They interpreted the current reversals in terms of different stability properties of the periodic rotating orbits and reported cases where current reversals also appear in the absence of a bifurcation from a chaotic to a periodic motion.

The class of inertial ratchets, in the absence of noise, may be related to the damped–driven pendulum, a chaotic system studied several years ago, among others, by Grebogi *et al* [22]. In

the case of the pendulum the state variable under study is the angle between the pendulum arm and the rest position, i.e. a S^1 type variable. In the case of a deterministic inertia ratchet the position of a particle in the periodic potential is an R^1 state variable. Then a periodic (chaotic) oscillation of the pendulum around the minimum corresponds to a regular (chaotic) movement of a particle in the periodic potential with zero mean velocity. An anticlockwise (clockwise) rotation of the pendulum corresponds to a movement of the particle in the ratchet potential with positive (negative) mean velocity.

The main difference between a deterministic inertia ratchet and a damped pendulum is the asymmetry in the potential. This asymmetry gives rise to a preferred direction of movement in the ratchet potential. Nevertheless, an important feature persists when the symmetry of the potential is broken: the fractal nature of the different coexisting attractors.

The problem of controlling the current reversal in inertia ratchets is important for technological applications, such as designing new particle separation techniques. We present in this work different strategies to control the current of an inertial ratchet. The control parameters analysed are the strength and frequency of the periodic external force, the strength of the quenched noise that models a non-perfectly-periodic potential, and the mass of the particles. For each control process the approach presented here is valid in regions in the control parameter's space where the ratchet has only two mean velocity attractors. Only noninteracting particles are considered. The success of each control mechanism is guaranteed by the fractal nature of the basins of attraction of these two mean velocity attractors. Then small perturbations of the control variable are enough to produce a jump between solutions with different net drift characteristics.

Another important issue for the actual realization of current control is the influence of disorder. In a recent work [15] some of us investigated the effect of quenched disorder on an underdamped rocking ratchet, finding that current reversal and chaotic diffusion may take place on otherwise regular trajectories and some chaotic trajectories become regular.

In the case of an overdamped ratchet subject to an external oscillatory drive, an unusual behaviour was reported in [11]: quenched disorder induces a normal diffusive transport in addition to the drift due to the external drive. Moreover, this diffusive motion is enhanced by higher values of the quenched disorder. If the quenched disorder has long-range spatial correlations, diffusion becomes anomalous, and both the correlation degree and the amount of quenched disorder can enhance the anomalous diffusive transport [20]. Understanding the origin of large fluctuations of the same order of magnitude as the average velocity is important from an experimental point of view, in studying friction, in investigating the motion of nanoclusters or monolayers sliding on surfaces, and in designing particle separation techniques.

Finally, we present the forced and overdamped motion of noninteracting particles in a periodic asymmetric potential [21]. The analysis is focused on synchronization of the motion of the particles with the external sinusoidal driving force. Two cases are considered: a perfect lattice without disorder and a lattice with noncorrelated quenched noise. The amplitude of the driving force and the strength of the quenched noise are used as control parameters. We show that the mean velocity of the particles and the diffusion coefficient have a nonmonotonic dependence on the quenched noise strength. We explain these nontrivial results on the basis of the synchronized motion of the individual particles in the perfect lattice.

2. The model

2.1. Single-particle systems

A single-particle inertial ratchet is modelled by the equation of motion:

$$\epsilon\ddot{x} + \gamma\dot{x} = -\frac{\mathrm{d}U}{\mathrm{d}x} + F(t) + G(x) \tag{1}$$

where ϵ is the mass of the particle, γ is the damping coefficient, U is the ratchet potential, $F(t)$ is the time dependent external force and $G(x)$ is the quenched noise. The external force is given by

$$F(t) = \Gamma \sin(\omega t) \tag{2}$$

where Γ and ω are respectively the amplitude and frequency of an external oscillatory forcing. The unperturbed ratchet potential is periodic and asymmetric and a typical function used to model it is

$$U(x) = -\sin(x) - \frac{\mu}{2}\sin(2x). \tag{3}$$

It has a period $\lambda = 2\pi$ and has been the subject of extensive studies both in models with [11, 15, 23] and without disorder [12–14]. The addition of the quenched disorder term

$$G(x) = \alpha\xi(x) \tag{4}$$

gives a more realistic representation of the substrate. The coefficient $\alpha \geqslant 0$ is the strength of this quenched disorder and $\xi(x)$ are independent, uniformly distributed random variables with or without spatial correlations, corresponding to a piecewise constant force on the period of the potential. Two special cases are

- overdamped ratchets, $\epsilon = 0$, and
- perfect lattice, $\alpha = 0$.

As usual in nonlinear dynamical systems, numerical solutions of equation (1) are required. Here they are obtained using a variable step Runge–Kutta–Fehlberg method [24].

To study the single-particle ratchet the evolution of several adimensional dynamical variables must be analysed because they give complementary information.

- The adimensional position $\tilde{x} = x/\lambda$; this gives the position of the particle along the ratchet.
- The adimensional velocity $\tilde{v} = v/v_\omega$, with $v_\omega = \lambda/T$. The mean value of this variable gives the transport velocity of a particle along the ratchet.
- The discrete sequences obtained by sampling $\tilde{x}$ and $\tilde{v}$ with a sampling period $T_{\mathrm{sa}} = T = 2\pi/\omega$:

$$\tilde{x}_{\mathrm{sa}} = \tilde{x}(kT)$$
$$\tilde{v}_{\mathrm{sa}} = \tilde{v}(kT) \qquad \text{with } (k = 0, 1, 2, \ldots).$$

  Using this variables it is easier to see if a synchronization with the external driving force has been reached.

A typical trajectory in an inertial ratchet consists of a transport movement, superposed on an oscillation. The transport movement may have $\langle\tilde{v}\rangle > 0$, $\langle\tilde{v}\rangle < 0$ indicating the transport sense. The particular case or $\langle\tilde{v}\rangle = 0$ indicates no transport along the ratchet. The oscillation may or may not be synchronized with the external driving force. The synchronization is recognized by a periodic sequence of $\tilde{v}_{\mathrm{sa}}$ and trajectories may be classified using their rotation number: if the movement along the ratchet becomes synchronized the rotation number is rational; if synchronization fails the rotation number is irrational.

Let us take an adimensional time $\tilde{t} = t/T$. A maximum value $\tilde{t}_{\mathrm{tran}}$ is defined to decide if synchronization has been reached or not. Then the permanent regime is considered to start at the first repetition of $\tilde{v}_{\mathrm{sa}}$ or at $\tilde{t}_{\mathrm{tran}}$, the first that occurs. After this starting point a trajectory is recorded up to $\tilde{t}_{\mathrm{max}}$, with $\tilde{t}_{\mathrm{max}} = \tilde{t}_{\mathrm{tran}} + N_{\mathrm{max}}$, where N_{max} is the period of the $\tilde{v}_{\mathrm{sa}}$ sequence in a synchronized case and it is an arbitrary value if no synchronization is reached.

The initial conditions are also relevant in nonlinear systems, in particular if several attractors coexist. In inertial ratchets the coexistence between two attractors with different mean velocities is interesting because it implies the possibility of controlling the transport along the ratchet to separate particles. Let us call these attractors *mean velocity attractors* and label them with the particle $\langle\tilde{v}\rangle$.

2.2. Multi-particle systems

To study the transport phenomena from a statistical viewpoint a collection of particles with different initial conditions is used. The collection of particles is represented by an ensemble consisting of N particles having initial velocities v_0 equally distributed in a range $[v_{\min}, v_{\max}]$, and initial positions equally distributed in the range $[x_{\min}, x_{\max}]$. The initial probability density is given by

$$\rho(\tilde{x}, \tilde{v}, 0) = [H(\tilde{v} - \tilde{v}_{\min}) - H(\tilde{v} - \tilde{v}_{\max})] \cdot [H(\tilde{x} - \tilde{x}_{\min}) - H(\tilde{x} - \tilde{x}_{\max})], \tag{5}$$

where $H(x)$ is the step function. The current is defined as

$$\langle\tilde{V}\rangle = \frac{1}{N}\sum_{i=1}^{N}\langle\tilde{v}\rangle_i.$$

To characterize the complete evolution of the packet, the first four adimensional cumulants, the adimensional mean velocity, and the adimensional diffusion coefficient of the sampled positions are evaluated as functions of the adimensional time. They are defined as follows:

$$\tilde{C}_1 = \langle\tilde{x}_k\rangle; \tag{6}$$

$$\tilde{C}_2 = \langle\tilde{x}_k^2\rangle - \tilde{C}_1^2; \tag{7}$$

$$\tilde{C}_3 = \langle\tilde{x}_k^3\rangle - 3\tilde{C}_1\tilde{C}_2 - \tilde{C}_1^3; \tag{8}$$

$$\tilde{C}_4 = \langle\tilde{x}_k^4\rangle - 4\tilde{C}_1\tilde{C}_3 - 6\tilde{C}_1^2\tilde{C}_2 - 3\tilde{C}_2^2 - \tilde{C}_1^4; \tag{9}$$

$$\tilde{V} = \lim_{t\to\infty} \mathrm{d}\tilde{C}_1/\mathrm{d}\tilde{t}; \tag{10}$$

$$\tilde{D} = \lim_{t\to\infty} \mathrm{d}\tilde{C}_2/\mathrm{d}\tilde{t}. \tag{11}$$

3. Control of transport properties

There are different possible strategies to control the current in a ratchet. In this paper we consider the strength and frequency of the periodic external force and the strength of the quenched noise. For each choice the approach presented here is valid in regions in the control parameter's space where the ratchet has only two mean velocity attractors. Only noninteracting particles are considered. The success of each control mechanism is guaranteed by the fractal nature of the basins of attraction of these two mean velocity attractors. Then small perturbations of the control variable are enough to produce a jump between solutions with different net drift characteristics.

Let us name generically η the selected control parameter. There are at least two different ways to do a real experiment to study the effect of η on the dynamics. One way is let the particle evolve starting from the same initial conditions when η changes (method I). Another possible way is to change η in the middle of the trajectory of the particle (method II). Simulations must be carried out with both methods because they give different information and they correspond to two possible experimental realizations. The interest is in collective behaviour, but when

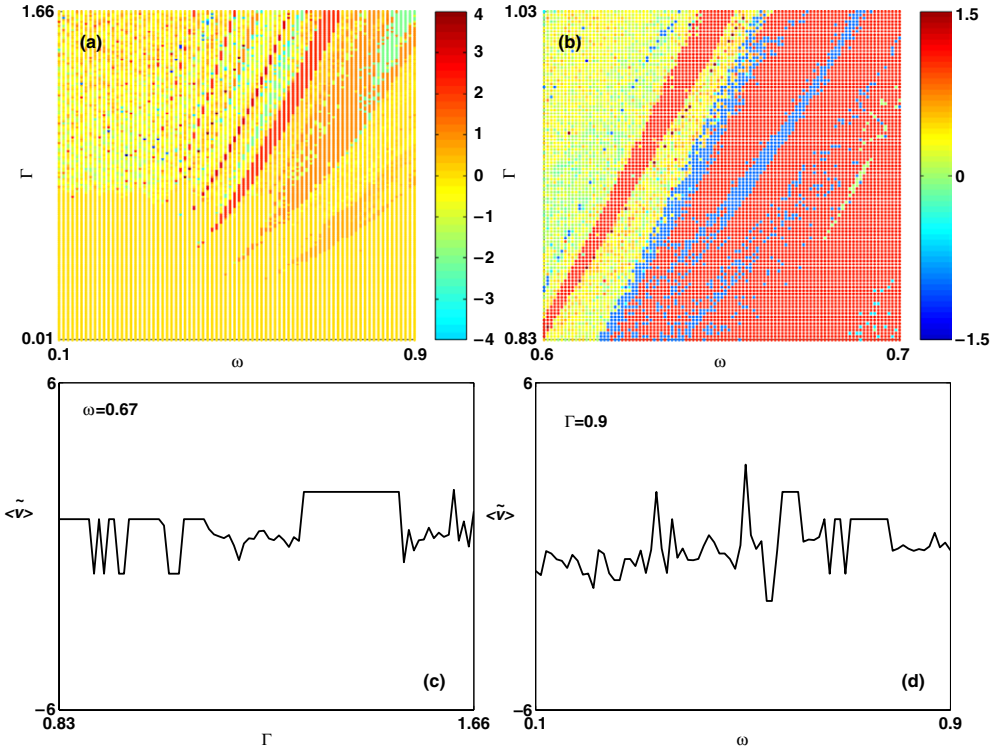

Figure 1. (a) Regions of different normalized mean velocities $\langle v\rangle/v_\omega$ in the parameter space (ω, Γ) obtained using method I. (b) Enlargement of the rectangle $\Gamma = [0.83, 1.03]$, $\omega = [0.6, 0.7]$. Intersection of the surface of figure (a) with the plane (c) $\omega = 0.67$, and (d) $\Gamma = 0.9$.

noninteracting particles are considered it is convenient to start the control procedure with the single-particle case. The control procedure will follow the following steps.

- *Step 1:* determine with method I a parameter's space region where two mean velocity attractors coexist.
- *Step 2:* verify with method II that two attractors coexist.
- *Step 3:* confirm that their domains of attraction are intermixed fractals.
- *Step 4:* check that the control is working in a few cases.
- *Step 5:* apply the control procedure to the multi-particle system.

4. Examples

4.1. Control by amplitude and frequency of the external driving force

4.1.1. Step 1. Determination of a region in the parameter space. Let us start with the case of a one-particle system ($\epsilon = 1.1009$) in a perfectly periodic potential ($\alpha = 0$), with $\mu = 0.5$ and damping coefficient $\gamma = 0.1109$. Consider the case of Γ and ω as control parameters.

To determine the region of interest in the parameter space we obtain the $\langle\tilde{v}\rangle$ bifurcation diagram using method I. If both control parameters, Γ and ω, are explored the parameters space is bi-dimensional. In figure 1(a) the regions of different normalized mean velocities are shown with different colours. See that inside the rectangle $\Gamma \in [0.83, 1.03]$, $\omega \in [0.6, 0.7]$,

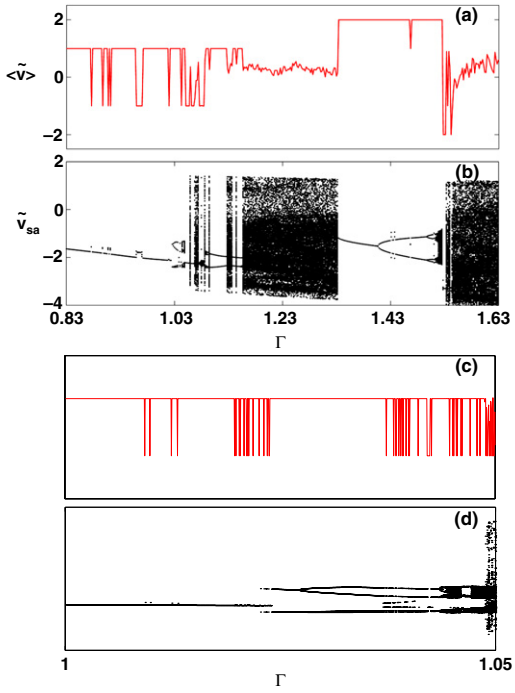

Figure 2. Bifurcation diagrams for a particle with initial conditions $\tilde{x}_0 = 0$, $\tilde{v}_0 = 1.5$ as a function of Γ, $\omega = 0.67$ by method I: (a) $\langle\tilde{v}\rangle$; (b) $\tilde{v}_{sa}$; (c) enlargement of (a) for $\Gamma \in [1, 1.05]$; (d) enlargement of (b) for $\Gamma \in [1, 1.05]$.

there are transitions between normalized mean velocities +1 and −1. The transitions may be more clearly seen in the enlargement of the rectangle, shown in figure 1(b), and they can also be seen in figures 1(c) and (d), where the intersections of the surface in figure 1(a), with the planes $\omega = 0.67$ and $\Gamma = 0.9$ are respectively shown. This is precisely a region of interest because these transitions are a hallmark of the coexistence of two mean velocity attractors.

Figure 2 shows both the adimensional mean velocity $\langle\tilde{v}\rangle$ (figure 2(a)) and the adimensional sampled velocity $\langle\tilde{v}_{sa}\rangle$ (figure 2(b)) bifurcation diagrams, with Γ as control parameter and $\omega = 0.67$. Figures 2(c) and (d) are enlargements for $\Gamma \in [1, 1.05]$. Let us make some remarks. (a) See again the inversions in $\langle\tilde{v}\rangle$ between the values +1 and −1 in the interval $\Gamma \in [0.83, 1.05]$ indicating the presence of two coexisting mean velocity attractors. (b) Note that there exists only one value of $\tilde{v}_{sa}$ in the same region. This fact indicates that the oscillations superimposed on the net transport motion are synchronized with the external driving force. (c) There are regions with several values of $\tilde{v}_{sa}$ but only one value of mean velocity: for example, in $\Gamma = 1.035\langle\tilde{v}\rangle = +1$, while $\tilde{v}_{sa}$ has four different values, indicating that the oscillations are synchronized with the external driving force but with a rotation number 1:4. Another interesting case is $\Gamma = 1.527$. In this case we have a chaotic oscillation superimposed on a transport motion with $\langle\tilde{v}\rangle = +1$. (d) The values of Γ where the inversions in $\langle\tilde{v}\rangle$ take place are strongly dependent on initial conditions. This a sign that the coexisting mean velocity attractor domains of attraction are intermixed fractals.

For a deep understanding, a few typical trajectories are shown in figures 3 and 4. In 3(a) and (b) we show the case of three trajectories corresponding to $\omega = 0.67$ and $\Gamma = 1.010$, $\Gamma = 1.011$ and $\Gamma = 1.015$ respectively. As can be seen in figure 1, all of them have only one

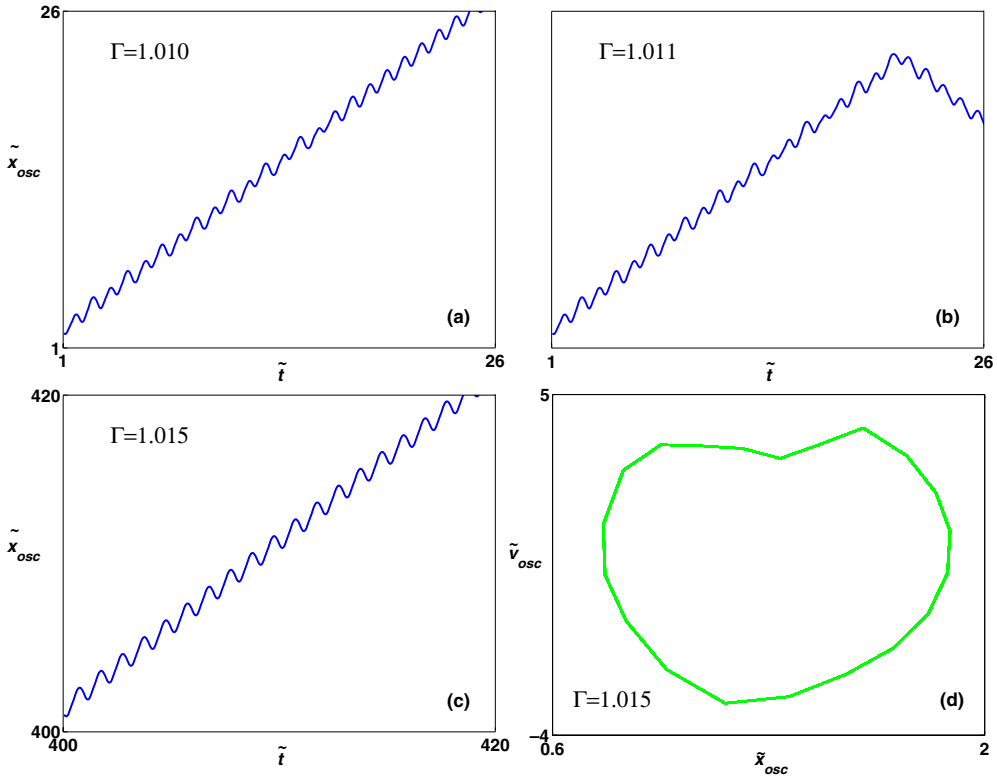

Figure 3. Trajectory of a particle with initial condition $\tilde{x}_{\rm osc} = 0, \tilde{v}_0 = 1.5$ for $\omega = 0.67$ and (a) $\Gamma = 1.010$, $\langle\tilde{v}\rangle = +1$ and $\tilde{v}_{\rm sa} \simeq -2$; (b) $\Gamma = 1.011$, $\langle\tilde{v}\rangle = -1$ and $\tilde{v}_{\rm sa} \simeq -2$; (c) $\Gamma = 1.015$, $\langle\tilde{v}\rangle = +1$ and $\tilde{v}_{\rm sa} \simeq -2$. (d) Typical phase space corresponding to oscillations superimposed on the net motion of particles of (a)–(c).

value for $\tilde{v}_{\rm sa} \simeq -2$, but they have $\langle\tilde{v}\rangle = +1$ or -1. The phase spaces corresponding to the oscillations superimposed on the net motion are similar and have rotation number 1, and its typical shape is shown in figure 3(d) for $\Gamma = 1.015$.

Figure 4 shows two more cases corresponding to $\omega = 0.67$ and $\Gamma = 1.035$ and $\Gamma = 1.527$ respectively. These trajectories correspond to regions of figure 2(d) where oscillations have different rotation numbers. For $\Gamma = 1.035$ the rotation number is 1:4, while for $\Gamma = 1.527$ oscillations are chaotic.

4.1.2. Step 2. Verifying the coexistence of two mean-velocity attractors with method II. Figure 5 shows the $\langle\tilde{v}\rangle$ bifurcation diagram obtained with method II. The step $\Delta\Gamma$ is 0.001 and the particle evolves during $\tilde{t} = 499$ for each Γ. Figure 5(a) was obtained beginning with $\Gamma = 0.896\,65$ as the initial Γ. The normalized mean velocity remains unchanged, equal to unity, until $\Gamma \simeq 1.05$. Figure 5(b) was obtained beginning with $\Gamma = 0.896\,66$ as the initial Γ. The normalized mean velocity remains unchanged at -1 until $\Gamma \simeq 1.08$. The initial Γs were chosen by looking at figure 2(c). For comparison figure 5(c) shows the bifurcation diagram with method I. A number of transitions take place between the two mean velocity attractors as Γ increases, showing that the system is extremely sensitive to the value of Γ. On the other hand, if method II is used the particle mean velocity remains locked to one of the attractors as Γ is changed. The locking value depends on the starting Γ.

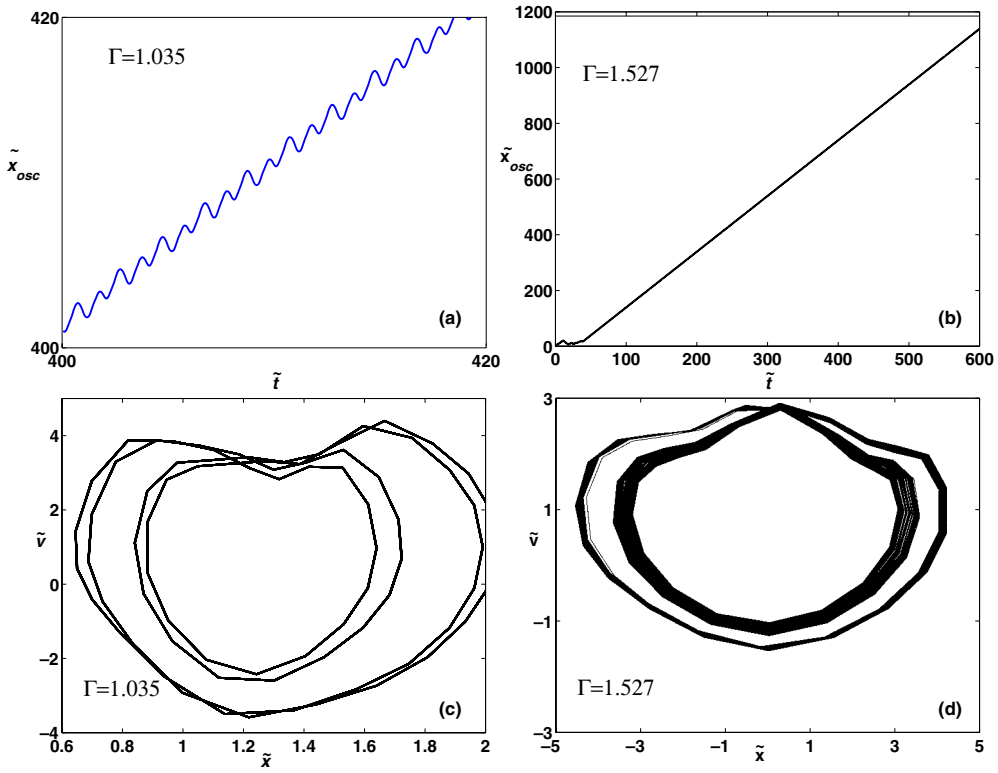

Figure 4. (a), (b) Trajectory of a particle with initial condition $\tilde{x}_0 = 0$, $\tilde{v}_0 = 1.5$ for $\omega = 0.67$ and (a) $\Gamma = 1.035$ and (b) $\Gamma = 1.527$; (c), (d) phase space corresponding to oscillations superimposed on the net motion of particles of (a) and (b).

4.1.3. Step 3. Confirming that the coexisting attractor domains of attraction are intermixed fractals. Extensive numerical simulations demonstrate that this behaviour in the parameter space is obtained when the domains of attraction of the coexisting mean velocity attractors are intermixed fractals.

To confirm this conjecture consider the case of Γ as control parameter, in the above mentioned range. We fixed $\epsilon = 1.1009$, $\gamma = 0.1109$, $\mu = 0.5$, $\Gamma = 0.896\,65$ and $\omega = 0.67$. The initial conditions are selected on a grid of 512×512 points in the rectangular region limited by $\tilde{x}_0 \in [-0.5, 0.5]$ and $\tilde{v}_0 \in [0, 2]$. These ranges are chosen to cover a whole spatial period for the potential (around the position $\tilde{x}_0 = 0$), and kinetic energies extending from zero up to the height of the potential barrier. As far as only two types of solution exist as discussed above, we denote with a black dot an initial condition (x_0, v_0) that leads to a trajectory with a normalized mean velocity -1, and we denote with a white dot an initial condition that leads to a trajectory with a normalized mean velocity $+1$. In this way, the basins of attraction for both mean velocity attractors were obtained, as shown in figures 6(a)–(d). Figures 6(b)–(d) are successive enlargements of figure 6(a) and the evidence of a typical fractal behaviour emerges from them. The solid lines in these figures are equipotential curves with the corresponding potential value printed on them. We used a box counting method to study the fractal nature of the mean velocity domains of attraction. Our results show that the mean velocity attractors are fractal with a dimension $d = 1.87$ for the negative mean velocity domain of attraction.

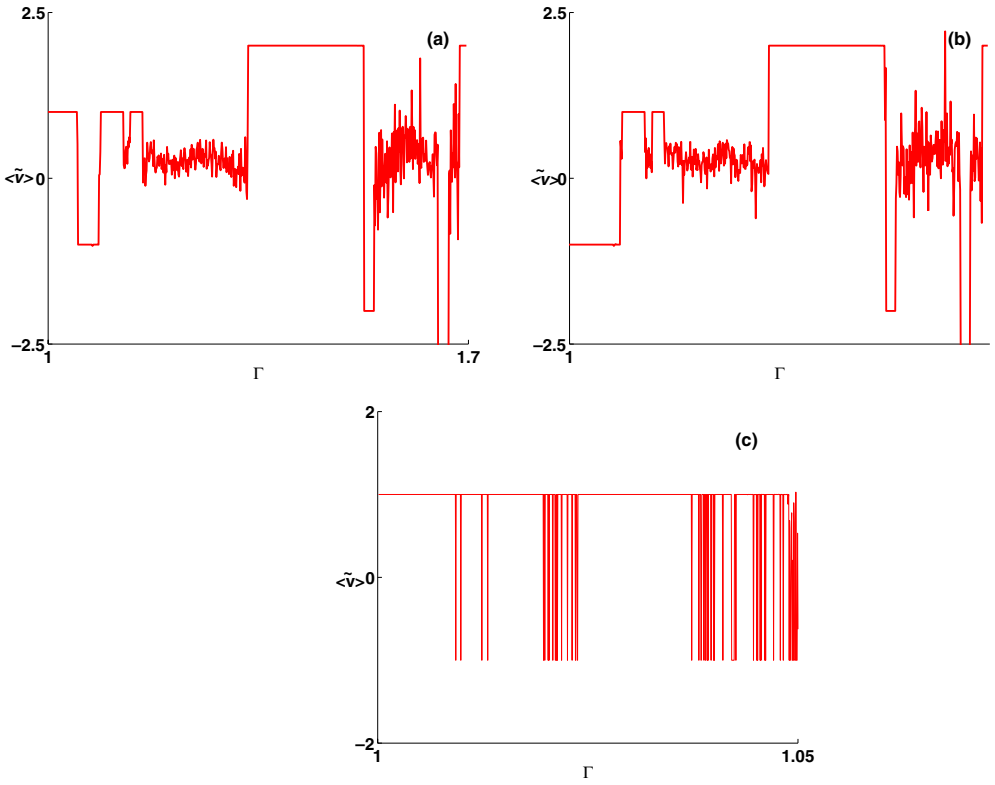

Figure 5. (a), (b) Normalized mean velocity bifurcation diagrams using method II. The particle has initial conditions $\tilde{x}_0 = 0$ and $\tilde{v}_0 = 1.5$. The control parameter is Γ, while $\omega = 0.67$. The particle starts at (a) $\Gamma = 0.896\,65$ and (b) $\Gamma = 0.896\,66$. (c) Bifurcation diagram using method I.

4.1.4. Step 4. Checking the control of the single-particle system. The practical consequence of having intermixed fractals is that most of the initial conditions belonging to the positive mean velocity domain of attraction are surrounded by initial conditions belonging to the negative mean velocity domain of attraction. Then it is possible to produce a jump from one attractor to the other using only a small perturbation in the value of Γ as shown in figure 7.

Several trials may be required to produce the desired jump but the important point is that only small perturbations are required. In a similar way the direction of movement may be reversed using a small change in ω.

4.1.5. Step 5. Controlling the current in a multi-particle ratchet. Let us consider the case of multi-particle noninteracting ratchets. As for the one-particle case we first show the results of simulations with method I, which in the packet of particles means returning to the initial condition $\rho(\tilde{x}, \tilde{v}, 0)$ when Γ changes.

The results shown in figure 8(a) were obtained with $N_{\max} = 200$, $[\tilde{x}_{\min}, \tilde{x}_{\max}] = [0.809, 1.83]$ and $v_0 = 1$ corresponding to a well spread-out packet of particles with initial positions between two maxima of the potential. There is only one current reversal at $\Gamma \simeq 1.05$, where an order–disorder transition takes place. About three-quarters of the particles in the ensemble have mean velocity $\langle \tilde{v} \rangle_i = -1$ and the remaining quarter have $\langle \tilde{v} \rangle_i = +1$, giving a normalized ensemble mean velocity $\langle \tilde{V} \rangle \simeq -0.5$. These results agree with Mateos's conjecture

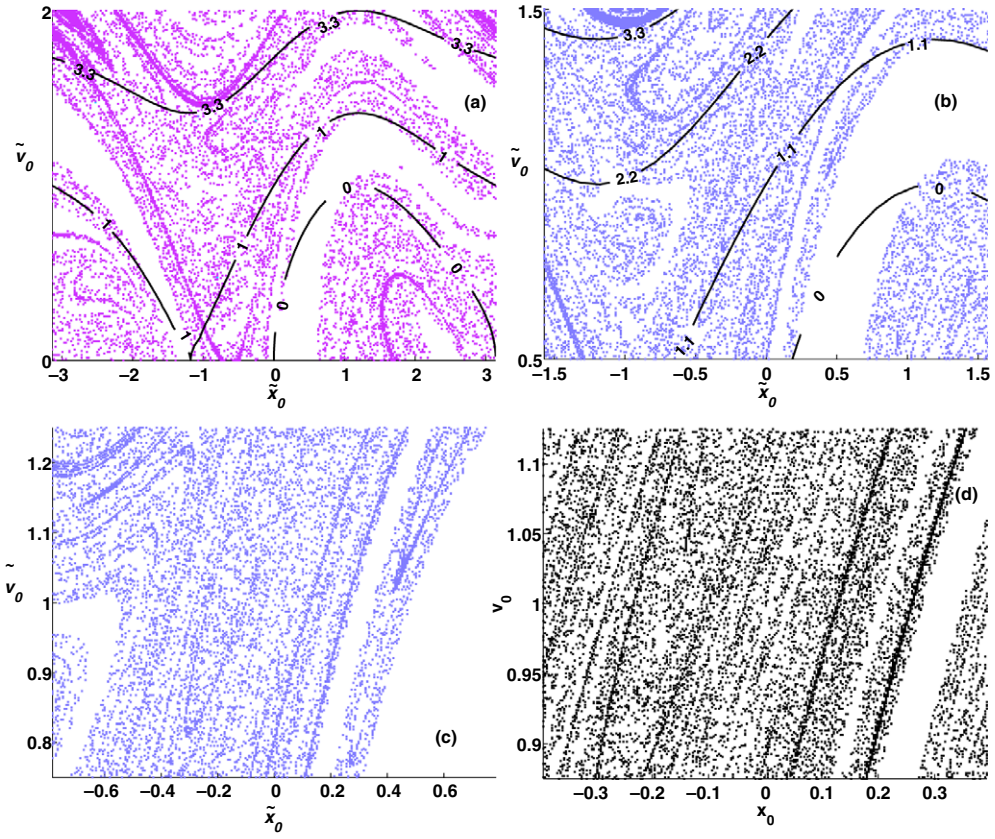

Figure 6. (a) Basins of attraction of $-v_\omega$ (black dots) and $+v_\omega$ (white dots) without quenched disorder ($\alpha = 0$) with $\Gamma = 0.896\,65$. The initial conditions are selected on a grid of 512×512 points. The solid lines are equipotential. (b)–(d) are successive enlargements of figure (a) to show the fractal nature of the basins of attraction.

that current inversion is associated with order–disorder transition in the bifurcation diagram of one particle [13].

In order to obtain the behaviour corresponding to a narrow initial packet, we work with the initial condition $[\tilde{x}_{\min}, \tilde{x}_{\max}] = [0.809, 0.810]$ and $v_0 = 1$. In this ensemble, particles are initially located near the maximum of the potential and having a small initial velocity. Figure 8(b) shows a current inversion around $\Gamma = 1.015$. The corresponding region at the bifurcation diagram has no order–disorder transition, contradicting Mateos's conjecture. However, the same current reversal, associated with an order–disorder transition, which was obtained for the case of a wide packet for $\Gamma \simeq 1.05$, does takes place.

Initial sets of particles with positions near the minimum of the potential and sets of particles with identical initial positions and different initial velocities equally distributed were also studied with qualitatively similar results.

It is possible to use method II to control the current. For example, to obtain a current $\langle \tilde{V} \rangle = -0.5$ which is the minimum current of figure 8(b), we use method II with the same narrow packet as used above, starting with $\Gamma_{\min} = 1.013$ and increasing it up to $\Gamma = 1.06$ in 100 equal steps. The time period for each step in Γ was commensurate with T. The normalized mean velocity as a function of Γ is shown in figure 8(c). As Γ changes each particle remains

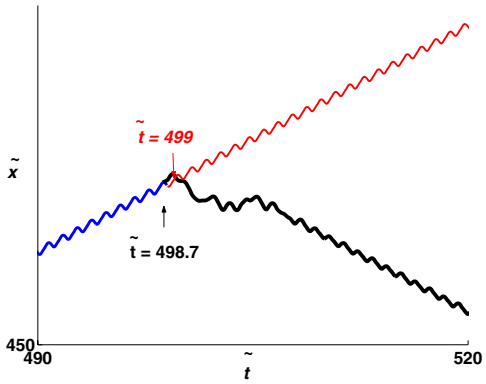

Figure 7. Example of control of current direction by selecting the time when Γ is changed from $\Gamma = 0.896\,65$ to $0.896\,66$. The bold curve corresponds to a changing time $t = 498.7T$. The thin curve corresponds to a changing time $t = 499T$.

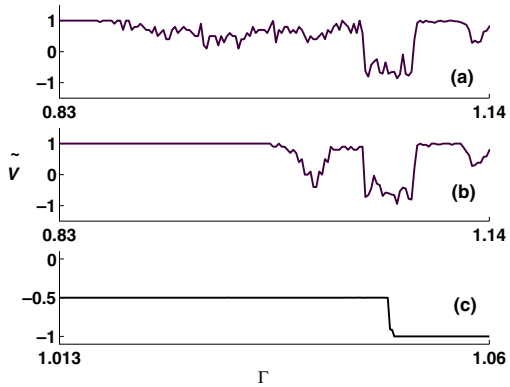

Figure 8. (a) Current of a set of particles with initial positions between two maxima of the potential $\tilde{x}_0 \in [0.809, 1.83]$ and initial velocity $v_0 = 0.01$ as a function of Γ (method I); (b) current of a narrow set of particles centred at the maximum of the potential ($\tilde{x}_0] \in [0.809, 0.810]$) and initial velocity $\tilde{v}_0 = 0.0067$ as a function of Γ (method I); (c) example of control of current; the narrow distribution of particles of (b) (method II).

locked to its mean velocity $\langle \tilde{v} \rangle_i$ corresponding to $\Gamma_{\min}$ and the current $\langle \tilde{V} \rangle$ also remains locked to its initial value -0.5. This behaviour persists until $\Gamma = 1.0495$, where the current drops to $\langle \tilde{V} \rangle = -1$. The unlocking effect corresponds to a chaos to order transition. If the simulation starts with any $\Gamma_{\min}$ producing a positive current for the packet, the unlocking effect produces a current reversal as Mateos found.

5. Control of the overdamped ratchet by the external driving force amplitude

Things are very different in the overdamped ratchet ($\epsilon = 0$). Let us start again with the case of only one particle with the specific initial condition $\tilde{x}_0 = 0$ and without quenched noise (i.e. $\alpha = 0$). Let us take $N_{\max} = 1200$. The bifurcation diagrams of $\tilde{v}_{\text{sa}}$ and $\langle \tilde{v} \rangle$ are shown in figure 9. Parameters are fixed to $\Gamma = 1$, $\mu = 0.5$ and $\epsilon = 0.1$ and two ranges of Γ are considered: $[0, 2]$ and $[2, 4]$.

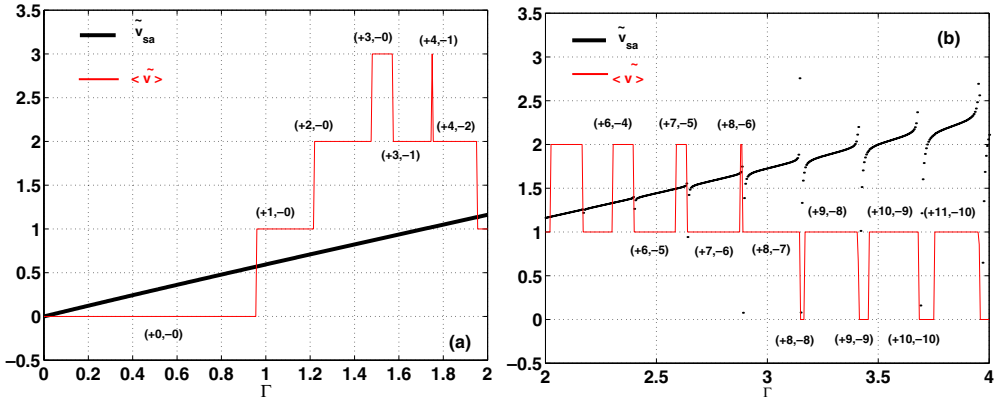

Figure 9. Adimensional sampled velocity $\tilde{v}_{sa}$, and mean velocity $\langle\tilde{v}\rangle$ of a particle in a perfect lattice, as a function of Γ. The particle starts at $\tilde{x} = 0$. (a) Note that for $\Gamma \in [0, 2]$ there are jumps in $\langle\tilde{v}\rangle$ at $\Gamma \simeq 0.96, 1.22, 1.47, 1.57, 1.75, 1.95$, but $\tilde{v}_{sa}$ has no bifurcations in this range of Γ. The label over each zone indicates the number of valleys crossed by the particle, forward (+) and backwards (−) in a period T. (b) $\Gamma \in [2, 4]$; jumps take place at $\Gamma \simeq 2.0125, 2.1675, 2.3025, 2.5875, 2.6375, 2.8775, 2.8875, 3.1475, 3.1675, 3.4125, 3.4575, 3.6825, 3.7525$ and 3.955; $\tilde{v}_{sa}$ bifurcates at the descending jump (i.e. for these values of Γ, $\tilde{v}_{sa}$ has more than one value).

For Γ values in the range $[0, 2]$ (figure 9(a)), $\tilde{v}_{sa}$ is a monotonic increasing function of Γ. On the other hand, $\langle\tilde{v}\rangle$ is a stepped function with jumps at specific Γ values. The reason for these jumps may be understood by considering how the particle's position $\tilde{x}$ varies with the adimensional time $\tilde{t}$. When Γ is below 0.96 the particle starts in a potential valley and it oscillates inside this valley in synchronism with the external drive returning to the same position and the same velocity every T. During the time T the particle stays inside the same valley at all times. This synchronism explains why only one value of $\tilde{v}_{sa}$ is obtained: every time the velocity of the particle is sampled it has the same value within its oscillatory motion. At $\Gamma = 1$ the particle starts in one valley of the potential; it moves uphill and ends in the same position but inside the forward contiguous valley. Therefore, over the region $\Gamma \in [0.96, 1.22]$ there is only one value of $\tilde{v}_{sa}$ but now $\langle\tilde{v}\rangle = 1$, showing that the particle remains synchronized with the external drive but now it advances one valley during T. As Γ increases the particle advances two valleys (see the label $(+2, -0)$ in figure 9(a)) and three valleys (see the label $(+3, -0)$ in figure 9(a)) during each T, giving $\langle\tilde{v}\rangle = 2$ and $\langle\tilde{v}\rangle = 3$, but it remains synchronized, giving only one value of $\tilde{v}_{sa}$. So far, the particle does not return to any valley during the driving-force negative semicycle. If Γ further increases, $\langle\tilde{v}\rangle$ presents descent jumps. The reason is that during T the particle goes forward crossing several valleys but it returns to one or more valleys during the negative semicycle of the external driving force. Moreover, the motion of the particle remains synchronized with the external force in the entire range $[0, 2]$ and $\tilde{v}_{sa}$ has only one value.

Let us now analyse the region $\Gamma \in [2, 4]$ shown in figure 9(b). Here $\langle\tilde{v}\rangle$ suffers many jumps between values 2 and 1 or between values 1 and 0. Furthermore, noninteger values of $\langle\tilde{v}\rangle$ may be obtained in these descent jumps. Two typical cases are $\Gamma \simeq 2.637$, where $\langle\tilde{v}\rangle = 4/3$ and $\tilde{v}_{sa}$ has three different values, and $\Gamma = 3.955$, where $\langle\tilde{v}\rangle = 6/7$ and $\tilde{v}_{sa}$ has seven different values. The discrete number of values for $\tilde{v}_{sa}$ indicates that the particle remains synchronized but now it starts in a valley and after T it ends in a different position inside another valley. For example, in the case $\Gamma \simeq 2.637$ the particle advances seven valleys and returns six valleys during T, but the last relative position is not equal to the initial one. Only after $3T$ does the particle reach the same relative position four valleys forward. This can be seen in a plot of the

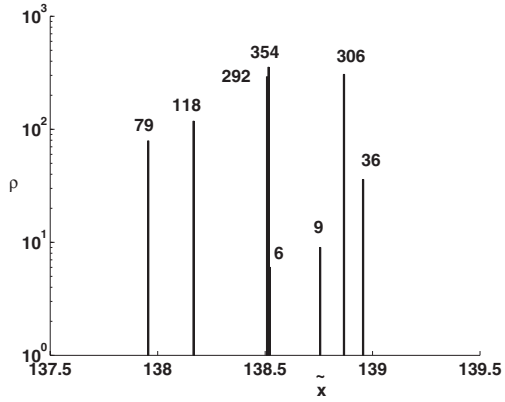

Figure 10. Particle distribution function for a packet of 1200 particles in a perfect lattice for $\Gamma = 3.955$ at $\tilde{t} = 160$. Initially, the particles are uniformly distributed over one valley, but the particles concentrate in eight bins at $\tilde{t} = 160$. The bins labelled 36 and 79 correspond to the same relative position in contiguous valleys.

phase space, $\tilde{v}_{\rm osc}$ as a function of $\tilde{x}_{\rm osc}$, where it can be seen that the phase-space curve closes itself after $3T$.

The situation is quite similar at all the other descending jumps. For example, at $\Gamma \simeq 3.955$, $\langle\tilde{v}\rangle = 6/7$ and $\tilde{v}_{\rm sa}$ has seven different values. After $7T$ the particle is in the same relative position but six valleys ahead of the initial one. The particle remains synchronized for every value of $\Gamma \in [0, 4]$ and then trajectories may be classified using their rotation number. For the descending jumps mentioned above, the rotation numbers of the trajectories are $1/3$ for $\Gamma \simeq 2.637$ and $1/7$ for $\Gamma \simeq 3.955$. The conclusion is that in overdamped ratchets particles remain locked to the external driving force.

To study the multi-particle system the evolution of the first cumulant $\tilde{C}_1$ is evaluated for different values of Γ, in the range $[0, 2]$. It increases linearly with time, changing its slope with Γ. Furthermore, all the higher order cumulants reach constant values and the adimensional diffusion coefficient $\tilde{D} = {\rm d}\tilde{C}_2/{\rm d}\tilde{t}$ drops to zero, after a very short transient (shorter than T).

We have also studied the evolution of the particle density with time. Initially, the particles are distributed over the whole valley, but the distribution collapses to only two positions as time evolves. In particular, it consists of two delta functions with most of the particles in one position inside one valley and a small number of particles located in the same relative position but inside the forward contiguous valley. As there are two delta functions and not only one, $\tilde{C}_2$, $\tilde{C}_3$ and $\tilde{C}_4$ are not equal to zero but they tend to a constant value. The diffusion coefficient $\tilde{D}$ is zero.

The situation is quite different at the bifurcation points of figure 9(b), for example $\Gamma \simeq 3.955$. In figure 10 the particle density function for this particular case is shown after $160T$. All the particles visit periodically seven positions inside a valley producing eight bins (two of them corresponding to congruent positions in two contiguous valleys). The first cumulant increases linearly with time with a fractional slope $6/7$ but all the other cumulants as well as the diffusion coefficient $\tilde{D}$ oscillate with an adimensional period equal to $7T$. A similar behaviour takes place for $\Gamma \simeq 2.637$, where $\tilde{C}_2$ and $\tilde{D}$ are $3T$ periodic functions of time and there are three positions inside each valley visited by the particles every $\tilde{t}_k$. Let us end the case of the perfect lattice remarking that the motion of the particles remains synchronized for all values of Γ and as a consequence only rational rotation numbers appear. There are no regions of interest in (Γ, ω) parameter space because there is no coexistence of mean velocity attractors.

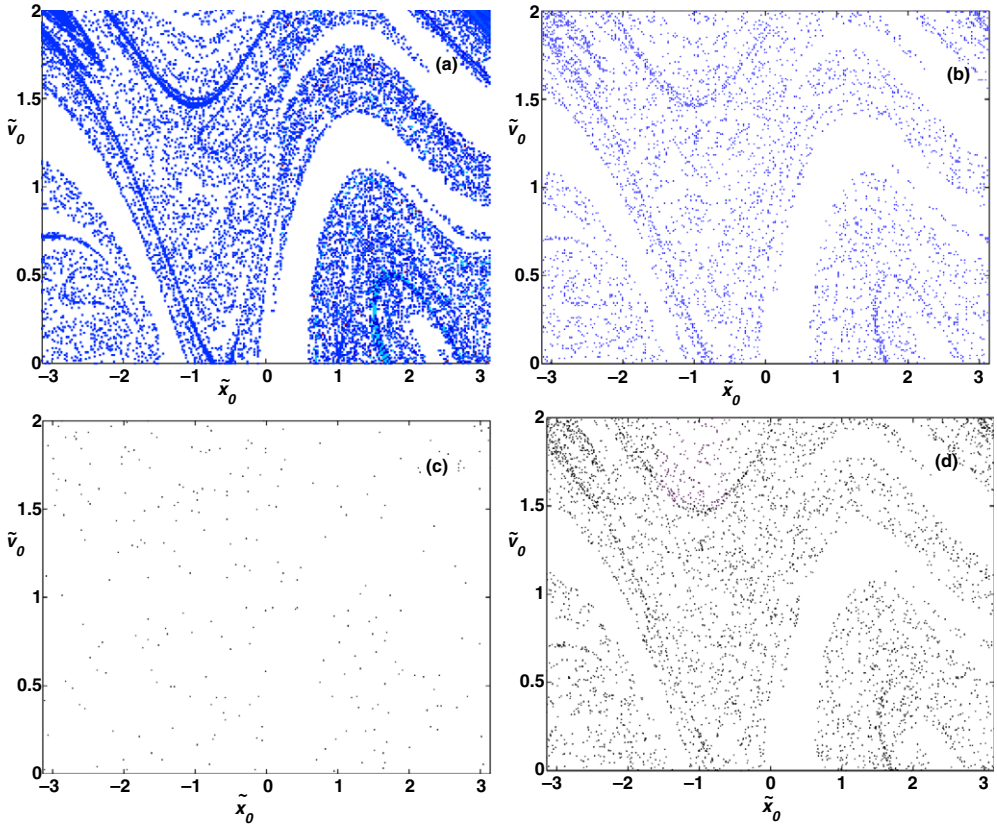

Figure 11. (a) Basins of attraction of $-v_\omega$ (black dots) and $+v_\omega$ (white dots) without quenched disorder ($\alpha = 0$) with $\Gamma = 0.896\,65$. The initial conditions of (a)–(c) are selected on a grid of 256×256 points. The initial conditions of (d) are selected on a grid of 1024×1024 points. (a) $\alpha = 0$, (b) $\alpha = 0.005$; (c) and (d) $\alpha = 0.008$.

5.1. The quenched noise as control parameter

5.1.1. Particles with mass. Let us start with the underdamped case with the same values as previously. An extensive numerical study is required to determine the way the quenched noise strength affects the structure of the domains of attraction; from $\alpha = 0$ up to $\alpha = 1$ was done. Some representative pictures corresponding to increasing values of α are shown in figure 11(a)–(c). Initial conditions are obtained from a grid of 256×256 points. The effect of increasing the quenched noise level is that the global shape of the domains is not modified, but the number of dots in the negative mean velocity attractor diminishes as α increases: the negative domain of attractions dissolves as α increases. In order to verify that the shape of the velocity domain remains unchanged, figure 11(d) shows the same strength of disorder as figure 11(b) but enlarging the number of initial conditions to a grid of 1024×1024 points.

All these figures show that the negative attractor dissolves as α increases. This result can be summarized in figure 12, where the function

$$P(\alpha) = \frac{N_-}{N_- + N_+}, \tag{12}$$

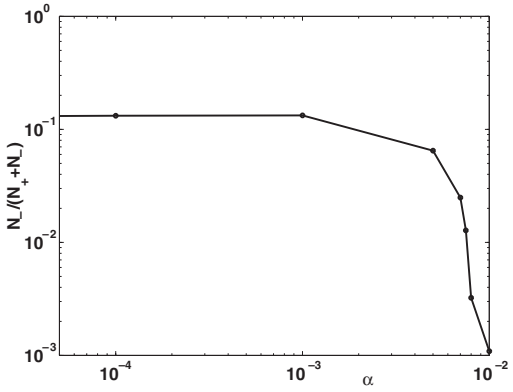

Figure 12. $P(\alpha)$ as a function of the quenched noise strength for $\Gamma = 0.896\,65$.

with $N_{\pm}$, the number of initial conditions corresponding to the ± 1 velocity domain, is plotted against α. This figure shows how the number of initial conditions in the domain of the negative mean velocity attractor dramatically diminishes for $\alpha \cong 0.0075$.

An interesting case is particles moving in inhomogeneous media. We work with an ensemble consisting of a hundred particles having identical initial velocities v_0 but initial positions equally distributed in the range $[x_{\min}, x_{\max}]$. The initial probability density is given by

$$\rho(x, v, 0) = \delta(v - v_0)[H(x - x_{\min}) - H(x - x_{\max})]. \tag{13}$$

The particles move in an inhomogeneous medium with two regions separated by an interface located at $x = 0$. Some representative results are shown in figure 13, where the stroboscopic normalized position of each particle is plotted as a function of the normalized time. Figure 13(a) shows the case with small quenched noise. The particles separate in two bunches moving with positive and negative mean velocities respectively. As the bunch going to the left enters the disordered medium it continues without any important effect.

As α increases, more and more particles initially going to the left are dispersed and reflected to the right, diminishing the negative current (figures 13(b) and (c)). This implies that α may be used as a control parameter of the positive and negative currents. For $\alpha \cong 0.008$ all the particles are finally moving to the right. The depth of penetration decreases as α increases over this value. Whenever a disorder threshold that depends on the mass of the particle is reached the localization effect [15] sets in. The localization may be seen in figure 13(d), where a high disorder strength is used and some particles are localized near zero.

5.1.2. The overdamped case. The control by quenched noise is specially interesting in the overdamped ratchet, where it may be studied from the point of view of synchronization. We are particularly interested in the influence of the quenched noise on $\langle \tilde{V} \rangle$ and $\tilde{D}$. As all the higher-order cumulants increase more slowly than $t^{n/2}$, $\rho(x, t)$ is asymptotically a Gaussian and it is determined by the first two moments only. For every value of the control parameters Γ and α we evaluate the positions of a packet of 200 particles, initially distributed over one valley. The cumulants and their derivatives, $\langle \tilde{V} \rangle$ and $\langle \tilde{D} \rangle$, are estimated by their value at $\tilde{t} = 500$ periods of the external driving force except in the cases $\Gamma = 2.5$ and $\Gamma \cong 2.637$, where $\tilde{t} = 10\,000$ was required.

We have studied the behaviour of the mean drift velocity $\langle \tilde{V} \rangle$, as a function of α for several values of Γ. The values of Γ were selected to show some of the typical situations that were

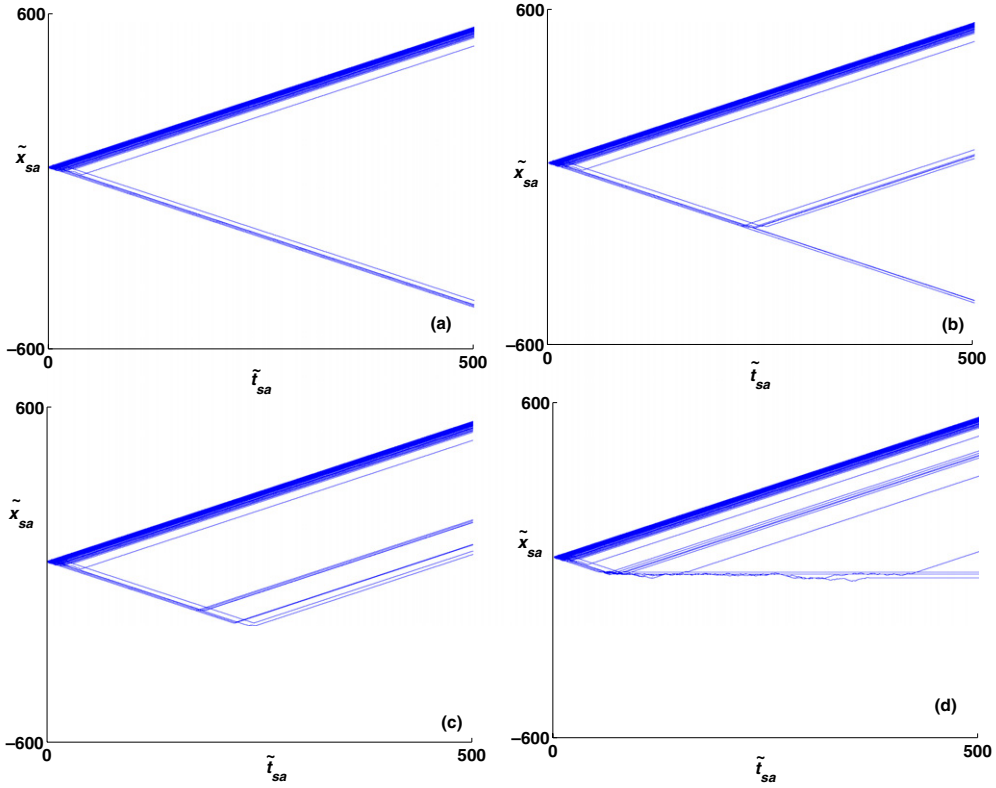

Figure 13. (a) Stroboscopic positions of an ensemble of 100 particles moving in an inhomogeneous medium. All the particles start with velocity $v_0 = 1$ and initial positions between $x_{\min} = 50\lambda$ and $x_{\min} = 51\lambda$. The region $x \geqslant 0$ has no spatial disorder. The region $x < 0$ has quenched disorder with strength α. (a) $\alpha = 0.001$, (b) $\alpha = 0.005$, (c) $\alpha = 0.008$ and (d) $\alpha = 0.6$.

found in our extensive numerical study. We note that, in some cases, noise enhances the drift motion, but in other cases it makes $\langle \tilde{V} \rangle$ decrease. Furthermore, for every Γ, there exists a specific threshold α_{th} over which $\langle \tilde{V} \rangle$ suddenly drops to zero. These characteristics may be explained for each curve of figure 14, on the basis of the synchronized motion in the perfect lattice (see figure 9), by the following procedure.

Step 1. Define $\Gamma_{\text{app}} = \Gamma + \alpha\xi(\tilde{x})$. In fact, only the extreme values of Γ_{app} are meaningful. They are $\Gamma_{\min} = \Gamma - \alpha$ and $\Gamma_{\max} = \Gamma + \alpha$.

Step 2. Using figure 9 determine the reachable synchronization zones, as well as the characteristic synchronized motion of the particles in each zone (this characteristic motion is resumed each zone label).

Step 3. Evaluate the allowed values for $\langle \tilde{v} \rangle$; they are determined by all the combinations of the differences between the positive and negative numbers in the labels of the reachable zones. These values determine if $\langle \tilde{V} \rangle$ will be an increasing or a decreasing function of α.

Step 4. The threshold value α_{th} is the minimum α making it possible for one of the allowed values of step 3 to be zero.

Note that every particle is affected by *different* values of Γ_{app} as it moves across different valleys of the potential. But in cases where the particles oscillate over several valleys it is convenient to define $\langle \Gamma_{\text{app}} \rangle^+$ as the time mean value of Γ_{app} during the positive semicycle and $\langle \Gamma_{\text{app}} \rangle^-$ as the time mean value of Γ_{app} during the negative semicycle.

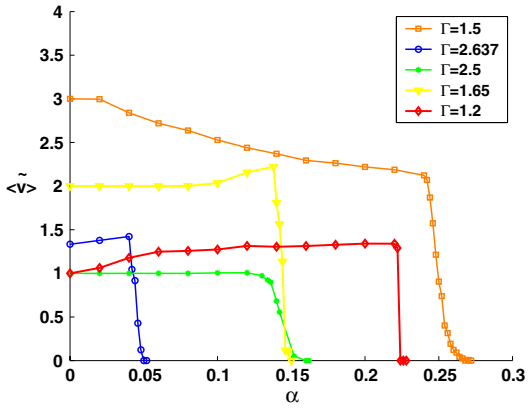

Figure 14. Adimensional mean velocity $\langle \tilde{V} \rangle$ as a function of α of the packet of particles. The curves corresponds to $\Gamma = 1.2$, 1.5, 1.65, 2.5, and 2.637.

Let us give the details for $\Gamma = 1.65$. This Γ value is in the synchronization zone $(+3, -1)$ in figure 1(a). For $\alpha < 0.08$, $\langle \Gamma_{\text{app}} \rangle$ may belong only to zone $(+3, -1)$. Then the only allowed value of $\langle \tilde{v} \rangle$ is 2 and $\langle \tilde{V} \rangle$ does not change. For $0.08 < \alpha < 0.10$, $\langle \Gamma_{\text{app}} \rangle$ may belong to zones $(+3, -1)$ or $(+3, -0)$. The only allowed values of $\langle \tilde{v} \rangle$ are 2 and 3. Consequently, $\langle \tilde{V} \rangle$ will be in between 2 and 3. This means that noise enhances the drift motion. For $0.10 < \alpha < 0.11$, $\langle \Gamma_{\text{app}} \rangle$ may belong to zones $(+3, -1)$, $(+3, -0)$ or $(+4, -1)$. The allowed values of $\langle \tilde{v} \rangle$ are 2, 3 and 4. Consequently, $\langle \tilde{V} \rangle$ continue increasing with α. For $0.11 < \alpha < 0.18$, $\langle \Gamma_{\text{app}} \rangle$ may belong to zones $(+3, -0)$, $(+3, -1)$, $(+4, -1)$ or $(+4, -2)$. The allowed values of $\langle \tilde{v} \rangle$ are 1, 2, 3 and 4. This means that according to the quenched noise found by the particle, it may increase or decrease its mean velocity. A statistical study of the probability of different quenched noise configurations will be reported elsewhere, showing that the value 1 is more probable than 2, 3 or 4, making $\langle \tilde{V} \rangle$ decrease. For $\alpha > 0.18$ region $(+2, -0)$ becomes reachable by $\langle \Gamma_{\text{app}} \rangle$ and localization appears. By the same arguments as above, traps will be two valleys long.

Let us analyse the characteristics of traps from another point of view. The superposition of the constant drift motion to an oscillation makes particles to move at variable speeds along the material, staying longer in those valleys located at both ends of their oscillation. Consequently, in spite of the zero spatial mean value of the force F produced by the ratchet potential,

$$\langle F \rangle_{\tilde{x}} = \int_{\tilde{x}_1}^{\tilde{x}_1+1} F(\tilde{x})\, \mathrm{d}\tilde{x} = U(\tilde{x}+1) - U(\tilde{x}) = 0, \tag{14}$$

the time mean value *felt* by the particles and given by

$$\langle F \rangle_{\tilde{t}} = \int_{\tilde{t}_1}^{\tilde{t}_1+1} F[\tilde{x}(\tilde{t})]\, \mathrm{d}\tilde{t} \tag{15}$$

will not be equal to zero but it is positive. In fact, this is the reason a sinusoidal force produces a drift when it is added to the ratchet potential.

Traps are several contiguous valleys with a negative quenched noise time mean value, that exactly compensates the positive time mean value of the ratchet potential force. When localization appears $\langle \tilde{V} \rangle$ falls to zero and the particles oscillate inside a small number of valleys, in synchronism with the external driving force. For example, for $\Gamma \cong 2.637$, $\langle F \rangle_{\tilde{t}} = +0.0366$. This small value may be obtained with α values as small as 0.05 as pointed in our analysis

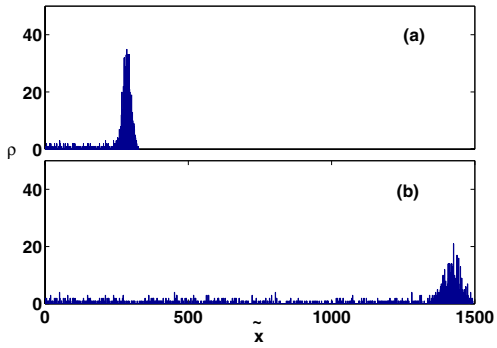

Figure 15. Distribution function of a packet of 1200 particles in a disordered lattice with $\alpha = 0.05$ for $\Gamma \simeq 2.637$. (a) $\tilde{t} = 200$; (b) $\tilde{t} = 1000$. The small bins in the particle density function are produced by localized particles.

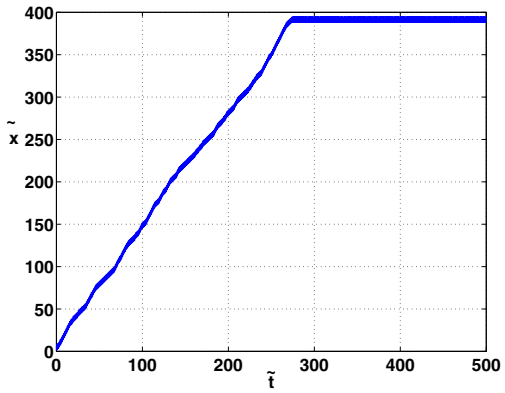

Figure 16. Particle trapped in a lattice with quenched noise $\alpha = 0.05$ for $\Gamma \simeq 2.637$. Adimensional position $\tilde{x}$ as a function of adimensional time $\tilde{t}$. The particle becomes trapped at $t \simeq 300$.

above. On the other hand, for $\Gamma = 1.65$, $\langle F \rangle_{\tilde{t}} \cong +0.15$. Then $\alpha \gtrsim 0.15$ is required for $\Gamma = 1.65$. This is again compatible with our synchronization analysis.

The evolution of the particle density $\rho(t)$ is shown in figure 15, with $\Gamma \cong 2.637$ and $\alpha = 0.05$. As time increases, more and more particles get trapped, diminishing drastically the value of $\langle \tilde{V} \rangle$. One of the localized particles is shown in figure 16 where the trap is in the region between valleys 388 and 394. In this region, the ratchet and noise forces felt by the particles are exactly cancelled by the time mean value of the quenched noise (remember that the driving force has zero time mean value). A trapped particle oscillates in synchronism with the external driving force. In the case of $\Gamma \simeq 2.637$ the oscillation covers a six-valley-long trap.

Let us now study the adimensional diffusion coefficient $\tilde{D}$ as a function of α. Diffusion is produced because quenched noise makes particles have different allowed mean velocities $\langle \tilde{v} \rangle$ instead of the only value allowed in the perfect lattice. Two typical cases are reported in figure 6: $\Gamma = 1.5$ (see figure 17(a)) and $\Gamma = 1.65$ (see figure 17(b)). For $\Gamma = 1.5$ localization does not appear in the α range considered, [0, 0.24]. The diffusion coefficient is an increasing function of α, indicating that diffusion is enhanced by noise because the range of allowed values of $\langle \tilde{v} \rangle$ enlarges with α. On the other hand, in the case $\Gamma = 1.65$, localization appears

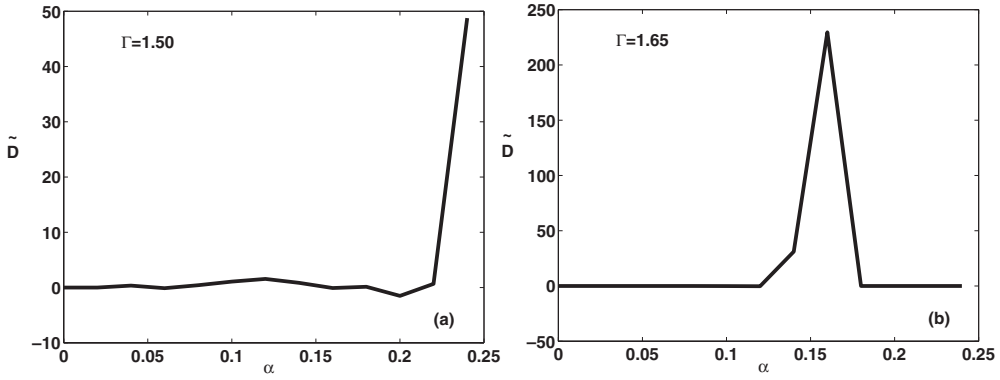

Figure 17. Adimensional diffusion coefficient $\tilde{D}$ as a function of α, for (a) $\Gamma = 1.5$ and (b) $\Gamma = 1.65$.

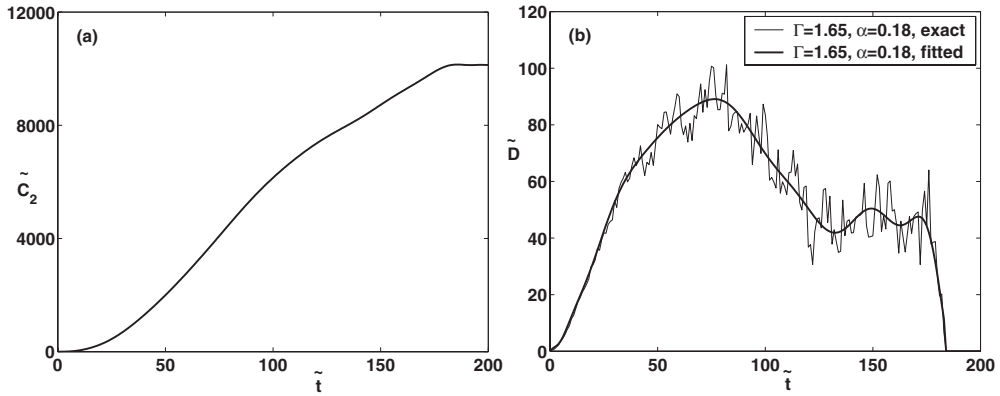

Figure 18. Typical time evolution of the second order cumulant and its derivative when localization exists. Here $\alpha = 0.18$ and $\Gamma = 1.65$. (a) Second adimensional cumulant $\tilde{C}_2$. (b) For $t \gtrsim 185$ all the particles become trapped and the adimensional diffusion coefficient $\tilde{D}$ is zero. The transitory evolution of $\tilde{D}(\tilde{t})$ depends on realization.

for $\alpha \geqslant \alpha_{\rm th}$, making $\tilde{D}$ decrease to zero. We would like to emphasize that in figures 14 and 17 $N_{\rm max} = 10\,000$ was needed in order to obtain a good estimate of $\langle \tilde{V} \rangle$ and $\tilde{D}$ over the entire range of values of Γ. The reason is that the transitory time $\tilde{D}$ becomes strongly dependent on realization, as demonstrated in figure 18, where we show plots of the typical time evolution of the second order cumulant and its derivative when localization exists, for $\alpha = 0.18$ and $\Gamma = 1.65$. Figure 18(a) shows the second adimensional cumulant $\tilde{C}_2$, and figure 18(b) shows that for $t \gtrsim 185$ all the particles become trapped and the adimensional diffusion coefficient $\tilde{D}$ is zero. Therefore, the transitory evolution of $\tilde{D}(\tilde{t})$ depends on realization. Thus, the transitory time for all the particles to be trapped considerably increases when localization with long traps is present.

6. Conclusions

Different strategies to control the current of deterministic ratchets, in the inertial and also in the overdamped limit, were reviewed in this work. The control parameters analysed in the inertial limit were the strength and frequency of the periodic external force, the strength of the

quenched noise that models a non-perfectly-periodic potential, and the mass of the particles. Control mechanisms are associated with the fractal nature of the basins of attraction of the mean velocity attractors. Small perturbations of the control variable may produce drift reversal. The analysis for the overdamped limit is focused on synchronization of the motion of the particles with the external sinusoidal driving force for two different substrates: a perfect lattice without disorder and a lattice with noncorrelated quenched noise. The amplitude of the driving force and the strength of the quenched noise were used as control parameters in the overdamped case.

Acknowledgments

This work was partially supported by UNMDP and ANPCyT. HAL is a CONICET researcher.

References

[1] Reimann P 2002 *Phys. Rep.* **361** 57
[2] Astumian R D 1997 *Science* **276** 917
[3] Astumian R D and Hanggi P 2002 *Phys. Today* **55** 33
[4] Feynman R P, Leighton R B and Sands M 1963 *The Feynman Lectures on Physics* (Reading, MA: Addison-Wesley)
[5] Ajdari A and Prost J 1992 *C. R. Acad. Sci. Paris* **315** 1635
Magnasco M O 1993 *Phys. Rev. Lett.* **71** 1477
[6] Daikhin L and Urbakh M 1994 *Phys. Rev.* E **49** 1424
Daly C and Krim J 1996 *Phys. Rev. Lett.* **76** 803
Ssorenseen M R, Jacobseen K W and Sstoltze P 1996 *Phys. Rev.* B **53** 2101
[7] Barabási A-L and Stanley H E 1995 *Fractal Concepts in Surface Growth* (Cambridge: Cambridge University Press)
[8] Zapata I, Bartussek R, Sols E and Hänggi P 1996 *Phys. Rev. Lett.* **77** 2292
[9] Gorre-Talini L, Sspatz J P and Silberzan P 1998 *Chaos* **8** 650
Derényi I and Astumian R D 1998 *Phys. Rev.* E **58** 7781
Ertas D 1998 *Phys. Rev. Lett.* **80** 1548
Duke T A J and Austin R H 1998 *Phys. Rev. Lett.* **80** 1552
[10] Hänggi P and Bartussek R 1996 *Lecture Notes in Physics* vol 476, ed J Parisi *et al* (Berlin: Springer)
[11] Popescu M N, Arizmendi C M, Salas-Brito A L and Family F 2000 *Phys. Rev. Lett.* **85** 3321
[12] Jung P, Kissner J G and Hänggi P 1996 *Phys. Rev. Lett.* **76** 3436
[13] Mateos J L 2000 *Phys. Rev. Lett.* **84** 258
[14] Barbi M and Salerno M 2000 *Phys. Rev.* E **62** 1988
[15] Arizmendi C M, Family F and Salas-Brito A L 2001 *Phys. Rev.* E **63** 061104
[16] Vale R D *et al* 2000 *Science* **288** 88
Endow S A *et al* 2000 *Nature* **406** 913
[17] Derényi I and Vicsek T 1996 *Proc. Natl Acad. Sci. USA* **93** 6775
[18] Lipowsky R and Jaster N 2003 *J. Stat. Phys.* **110** 1141
[19] Hondou T and Sawada Y 1995 *Phys. Rev. Lett.* **75** 3269
[20] Gao L, Luo X, Zhu S and Hu B 2003 *Phys. Rev.* E **67** 062104
[21] Zarlenga D G, Larrondo H A, Arizmendi C M and Family F 2005 *Physica* A **352** 282
[22] Grebogi C, Ott E and Yorke J A 1987 *Science* **238** 585
[23] Larrondo H A, Family F and Arizmendi C M 2002 *Physica* A **303** 78
[24] Press W H, Teikolsky S A, Vetterling W T and Flannery B P 1995 *Numerical Recipes in C* (Cambridge: Cambridge University Press)